Indian Journal of Pure & Applied Physics
Vol. 61, February 2023, pp. 96-101
DOI:

Investigation of Optical Properties of Nanostructured $Ce_{0.80-x-y}Nd_xTb_yO_2$ Compound

Handan Ozlu Torun[a]*, Rabia Kırkgecit[b] , Esra Ozturk[c] & Fatma Kılıc Dokan[d]

[a]Department of Energy System Engineering, Kahramanmaraş İstiklal University, Kahramanmaraş, 46300, Turkey

[b]Institute of Science, Material Science and Engineering, Kahramanmaraş Sütçü İmam University Kahramanmaraş, 46050, Turkey

[c]Department of Metallurgical and Materials Engineering, Karamanoglu Mehmetbey University Karaman, Turkey

[d]Department of Chemistry Processing Technologies, Kayseri University, Kayseri, Turkey

Received 11 October 2022; accepted 18 January 2023

In this study, the sol-gel method synthesized nano-structured $Ce_{0.80-x-y}Nd_xTb_yO_2$ compounds that can be used in optoelectronic devices. In the characterization studies of the synthesized compounds, XRD, FE-SEM-EDX, TG-DTA, Raman, and photoluminescence spectrophotometer were used. The thermal analysis determined that the degrading species were removed at 600 °C and cubic crystalline compounds were obtained according to the XRD data. EDX data confirmed the presence of host and activator elements in the compound. It was determined that oxygen vacancy formation was more intense in the 5% Nd-15%Tb doped compound. According to these results, 5% Nd phosphorus-doped $Ce_{0.80-x-y}Nd_xTb_yO_2$ was reported to be a good candidate for optoelectronic applications where both red and green photoluminescence are required in the same crystal.

Keywords: CeO_2; Optoelectronic; Sol-gel

1 Introduction

CeO_2 is a rare earth metal oxide compound in the lanthanide group. CeO_2 is one of the most abundant metal oxide compounds in nature. In addition, its chemical and physical properties have enabled it to be used in a versatile area. The most prominent of these can be listed as follows; ceramic electrolytes[1], luminescent materials[2], photocatalysts [3], and sensors [4].

CeO_2 is a natural luminescent material with an ideal host matrix in its crystal structure, with a reduction between $Ce^{4+/}Ce^{3+}$ and oxygen ion vacancies and 4f orbital[5,6]. The high luminescence efficiencies of rare earth element-doped CeO_2 compounds are significant in biological staining, medical imaging, and defense. So far, the physical and chemical results of CeO_2 luminescent materials created with the contribution of some elements have been reported. Kunimi and Fujihara found that Pr-doped CeO_2 and (Pr, Eu)codoped compounds have red radiation[7]. Fujihara and Oikawa investigated the luminescence behavior of thin films of Sm and Eu-doped CeO_2 compounds[8]. Yoshida, and Fujihara, examined the optical change of the nanostructured CeO_2:Sm compound according to its structural properties and found that it emits orange-red radiation[9]. Singh *et al*. In optical studies of (Er) and (Er, Yb) doped CeO_2 compounds, they reported that the radiation intensity and intensity were better in the co-doping compound, and they obtained red-green radiation[10]. Balestrieri *et al*. investigated the (Nd, Yb, Sm, Pr)-doped CeO_2 luminescence behaviors according to the additive types. They observed different spectral transitions for each additive type[11]. Choudhury *et al*. reported the results of the spectral regions and oxygen defects in CeO_2 compounds according to the amount of Nd in their research[12]. Recently, luminescent materials with red radiation have gained importance and are being intensively researched[13-15]. Wang *et al*. investigated the optical properties of CeO_2:Eu^{3+}(Sm^{3+}, Tb^{3+}) compounds. They reported the presence of intense red radiation[16]. Malleshappa *et al*. investigated the luminescence of CeO_2:Tb^{3+} compound according to Tb additive amount. They observed radiation in the green zone[17].

When the previous studies have been examined, there are studies on the optical properties of (Nd)-doped CeO_2 and (Tb)-doped CeO_2 compounds, but the optical properties of (Nd, Tb) co-doped CeO_2 has

*Corresponding author:
(E-mail: handan.ozlutorun@istiklal.edu.tr)

not been reported yet. Therefore, in this study, the structures of $Ce_{0.80-x-y}Nd_xTb_yO_2$ compounds obtained by the co-doping method were elucidated, and the changes in their optical properties were examined according to Nd contribution.

2 Materials and Method

The sol-gel method was used for the synthesis of $Ce_{0.80-x-y}Nd_xTb_yO_2$ compounds. As starting compounds, cerium (III) nitrate hexahydrate ($Ce(NO_3)_3{\cdot}6H_2O$), terbium (III) nitrate hexahydrate ($Tb(NO_3)_3{\cdot}6H_2O$), neodymium (III) nitrate hexahydrate ($Nd(NO_3)_3{\cdot}6H_2O$) were determined. 5% Nd-15% Tb, 10% Nd-10% Tb and 15%Nd-5% Tb were determined as doping rates. Compounds calculated according to mole percent ratios were first dissolved in distilled water. Ethylene glycol and citric acid were added to the clear solution. It was heated until it was gelling. Pre-drying was done at 150 °C. Then heat treatment was carried out at 600 °C for 8 hours.

The crystal properties of the synthesized photocatalysts were examined via X-Ray diffraction (XRD) (Pananalytic Imperial X-Ray diffractometer). The XRD pattern measurements of all samples were taken using a 0.02° step angle in the range of 2θ = 10-90°, at 40 kV and 40 mA. The XRD powder pattern was indexed using HighScore Pro software, and the unit cell parameters were calculated. Thermal properties were investigated using a Perkin Elmer TG-DTA analyzer. A portable Raman spectrometer (BWS465 B.W. Tech. Inc.) with 1300-100 cm^{-1} 785 nm He-Ne laser was used to examine the movements of the molecules and the degradations in the structure due to the vibration of the synthesized powder particles. The surface morphology of the compounds was investigated using field scanning electron microscopy (FE-SEM) (Zeiss), and elemental analysis was carried out via energy-dispersive X-ray spectroscopy (EDX). Optical properties were examined with a Fluorescence spectrophotometer (HITACHI F-7100) All PL measurements were performed in an open atmosphere and at room temperature.

3 Result and Discussion

3.1 Thermal Analysis

The TG graphs of the samples taken after pre-drying, which is the synthesis step of the compounds, are given in Fig. 1. As can be seen, a three-stage TG curve is seen in the formation of

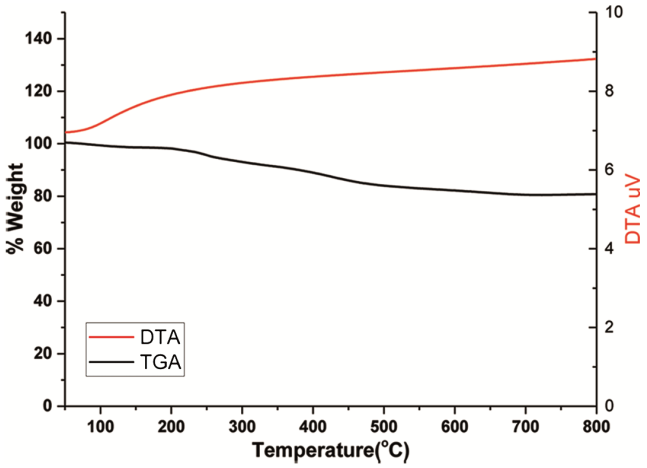

Fig. 1 — Thermal Degradation of $Ce_{0.80-x-y}Nd_xTb_yO_2$: % 5Nd% 15Tb.

the desired compound. the reaction that takes place in the preparation of the compounds can be predicted as follows[18]:

$$1\text{-x-y}Ce(NO_3)_3 \setminus (aq) \setminus + yTb(NO_3)_3\ (aq) + xNd(NO_3)_3\ (aq) + C_6H_8O_7\ (aq) \rightarrow$$

$$Ce_{1-x-y}Nd_xTb_yO_2 + 6CO_2\ (g) + 4H_2O\ (g) + 3(1\text{-x-y})\ N_2$$

The change in the TG curve is the removal of non-molecular water in the first step, while the molecular water in the other steps, the decomposition of nirtars, and the complete combustion of the organic compound to form CO_2. As can be seen, the decomposition has been completed at the selected sintering temperature.

According to the DTA signals, it can be seen that there is no phase change at the selected sintering temperature and that it remains stable.

3.2 Crystal Structure Analysis(XRD)

In general, x-ray powder diffractometry is a technique used in crystal structure illumination. The sintering temperature was determined as 600 °C using the thermal analysis curves in the synthesis processes. The XRD analysis patterns performed after 8 hours of sintering are given in Fig. 2. The diffraction peaks comply with ICDS − 98–015-5608. They are obtained by cubic crystal lattice compound. The physical parameters obtained as a result of the evaluations of the compounds using the diffraction peaks are summarized in Table 1. As can be seen, the lattice parameters change with doping at different rates. This change can be explained by the additive ions' radius difference. The eight-coordinated radii of Nd^{3+} and Tb^{3+} ions are 1.109 Å and 1.04 Å. Ce^{4+} is 0.97 Å[19]. As can be seen in Table 1, the lattice parameter increased

as the Nd amount increased. Because $r_{Nd+3}>$ is r_{Tb3+}. In addition, the slight shift in the peaks observed when compared with 5% Nd and 15% doped in the (111) plane family is due to the increase in the Nd^{3+} ion radius. Generally, if the radius of the doped ion is large, it will cause the lattice structure to expand[20].

The crystal structure properties of the synthesized compounds were determined by using the data in HighScore Pro software and the Debye-Scherrer Eq. 1 was calculated.

$$D= k\lambda/\beta.\cos\theta \quad \ldots (1)$$

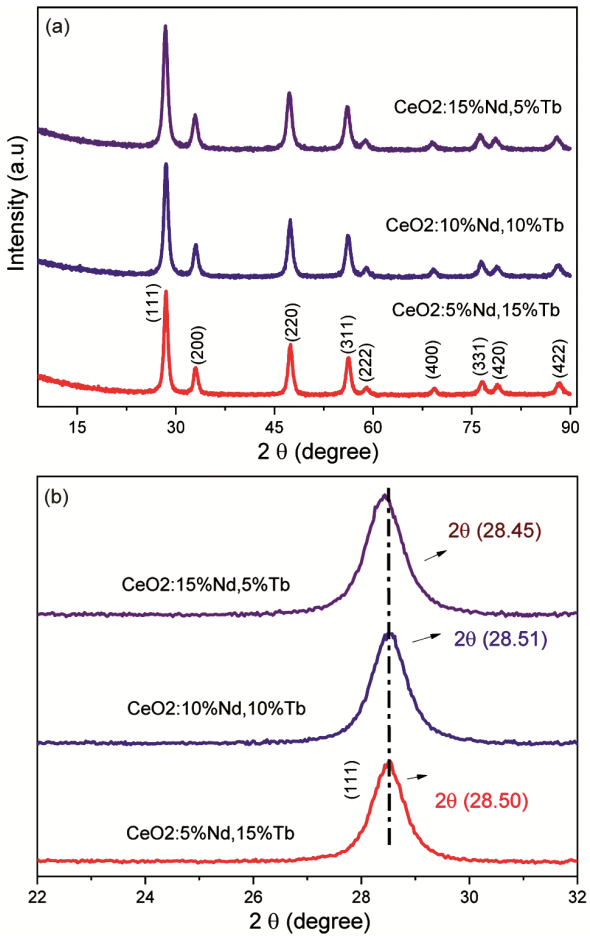

Fig. 2 — X-ray powder diffraction pattern of compounds after 8 hours of heat treatment at 600 °C.

Where-β- full width at half maximum (FWHM) of the diffraction peak, λ-wavelength (1.5418), θ-Bragg's-angle, and k-Scherrer constant (0.88–0.92).

Determination of crystal structure properties is important for luminescence applications. When the data in Table 1 are examined, it is seen that nano-sized compounds were obtained.

3.3 Raman Analysis

Raman analysis is widely used to study oxygen formation in the crystal structure of fluorite CeO_2. According to Fig. 3, The peak of 464 cm^{-1} belonging to the pure CeO_2 compound belongs to the F2g vibration with a typical fluorite structure[21]. This vibrational mode is dependent on the movement of oxygen. With doping, shifts in the band structure and, in addition to this, new bands of 550 cm^{-1} and 600 cm^{-1} are observed. This indicates a defect in the crystal structure by doping. In general, the band at 550 cm^{-1} and 600 cm^{-1} is attributed to oxygen vacancy formation[22,23]. It is possible to say that oxygen ion vacancy formation is more in the 5% Nd doped compound due to the high peak density at 550 cm^{-1}. The effect of these data on the radiation properties in Raman is explained.

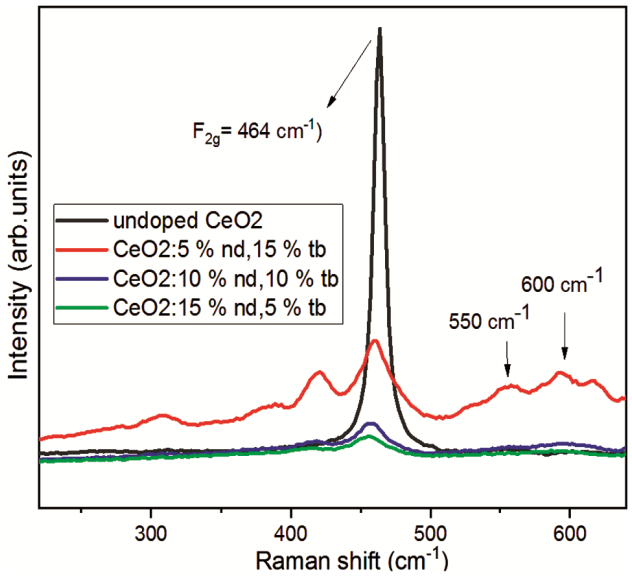

Fig. 3 — Raman spectra for $Ce_{0.80-x-y}Nd_xTb_yO_2$.

Table 1 — Crystal Structure properties of $Ce_{0.80-x-y}Nd_xTb_yO_2$

Samples	Lattice parameters	Volume	Crystalline size (nm)				Micro strain (%)			
	a (Å)	$(Å)^3$	Mean value	(111)	(022)	(113)	Mean value	(111)	(022)	(113)
CeO2:15%Nd,5%Tb	5.438	160.86	9.83	11.19	8.62	8.64	0.35	0.39	0.34	0.29
CeO2:10%Nd,10%Tb	5.427	159.84	11.23	12.37	9.76	10.47	0.38	0.38	0.39	0.37
CeO2:5%Nd,15%Tb	5.422	159.39	12.98	13.94	11.59	11.54	0.41	0.44	0.42	0.33

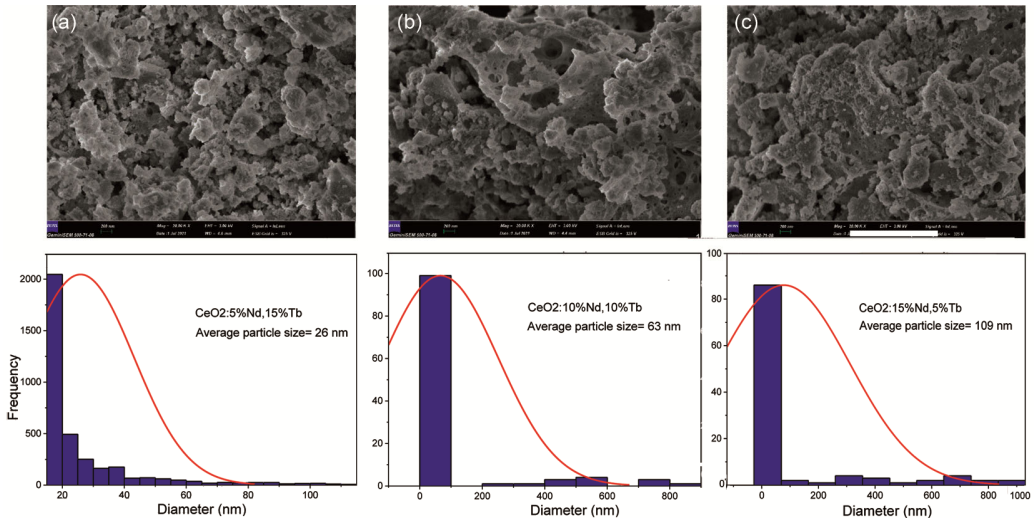

Fig. 4 — (a) FESEM images and size distribution histogram for CeO_2:5%Nd,15%Tb samples; (b) FESEM images and size distribution histogram for CeO_2:10%Nd,10%Tb samples; (c) FESEM images and size distribution histogram for CeO_2:15%Nd,5%Tb samples.

3.4 Morphological Characteristics: FE-SEM/EDX

The surface morphology and particle sizes of the compounds, which were heat treated at 600 °C for 8 hours, were investigated by FE-SEM. Images of these compounds are given in Fig. 4 a,b,c. The histograms obtained from these images determined that the particles changed in sizes of 26-109 nanometers. Particle shapes were found to be similar for all three compounds. It was determined that the 5% Nd doped compound had the lowest particle structure. As seen in the EDX graphics in Fig. 5, host and activator ions are located in the crystal structure of three different compounds.

3.5 Photoluminescence Properties (PL)

The photoluminescence spectra of $Ce_{0.80-x-y}Nd_xTb_yO_2$ doped with 5%, 10% ve 15% Nd^{3+} phosphors are shown in Fig. 6. All phosphors have an excitation band belonging to the charge transfer band (CTB) at 260 nm[24,25] and no excitation bands of Tb^{3+} or Nd^{3+} ions were observed. Nd^{3+} ions used as dopants are excited between 500-900 nm and emit at longer wavelengths[26]. Therefore, there is no excitation or emission band of Nd^{3+} ions in the PL spectrum. The issue here is how Nd^{3+} ions affect the radiation of Tb^{3+} ions. It is seen in the emission spectrum in Fig. 6 that when the doping ratio of Nd^{3+} ions is 15%, the emission band originating from the $_5D^4 \rightarrow {}_7F^5$ transition of Tb^{3+} ions is obtained at 530 nm in the green region of the spectrum[27]. The same emission band is also observed when the doping ratio of Nd^{3+} ions is 5% and 10%. For 5% and 10% Nd^{3+} doping ratios, the important point is that in addition to the

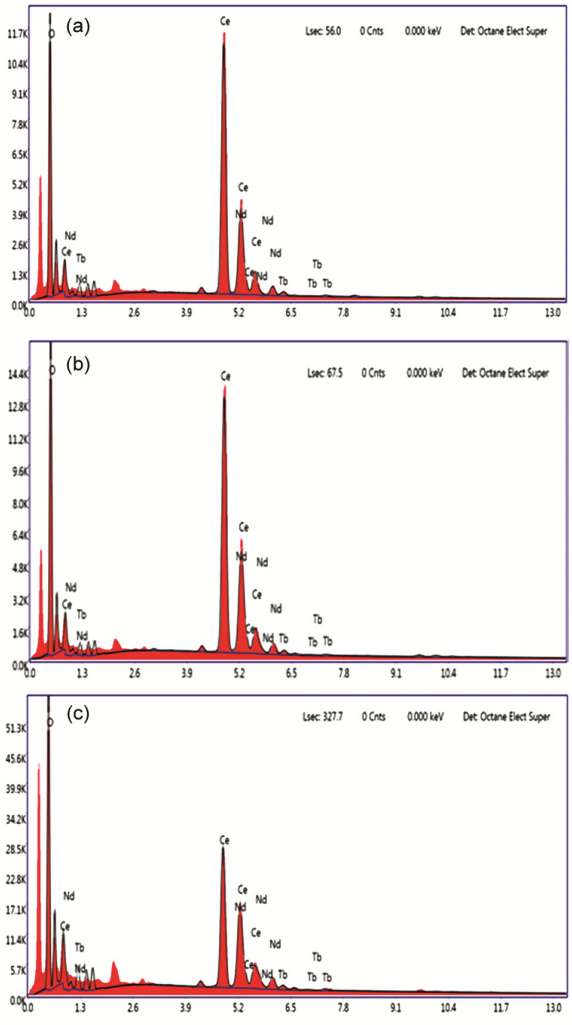

Fig. 5 — EDX analysis for (a) CeO_2:5%Nd, 15%Tb (b) CeO_2:10%Nd, 10%Tb (c) CeO_2:15%Nd, 5%Tb.

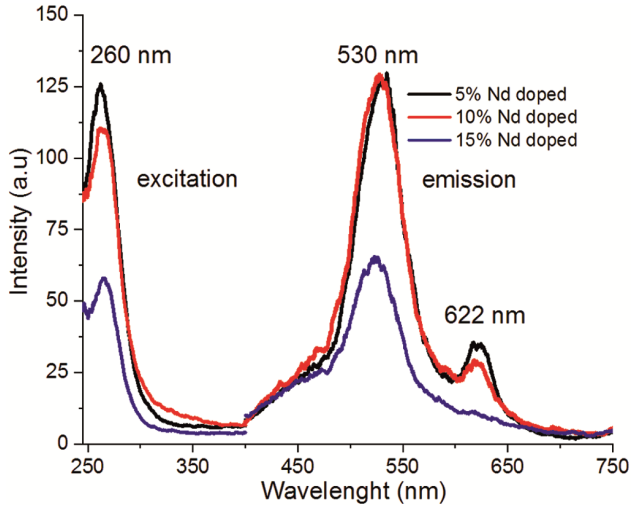

Fig. 6 — The photoluminescence spectra of $Ce_{0.80-x-y}Nd_xTb_yO_2$ doped with 5%, 10% ve 15% Nd^{3+} phosphors.

green emission at 530 nm, a red emission band corresponding to the $_5D^4 \rightarrow {}_7F^3$ transition of Tb^{3+} ions at 622 nm is also obtained. When the 5% and 10% Nd^{3+} doping ratios are compared, it is seen that the red emission band at 622 nm has a higher intensity for the 5% Nd^{3+}doping ratio, although the intensity of green emission bands at 530 nm does not change. According to the photoluminescence spectrum in Fig. 6, the green region emission given by the Tb^{3+} ions in the CeO_2 crystal can be extended to the red region by doping Nd^{3+} ions and the optimum doping ratio of Nd^{3+} ions is 5%. % As a matter of fact, the results of Raman and FESEM analysis also support the photoluminescence results. As can be seen in Fig. 3 according to the Raman analysis, the highest oxygen ion vacancy was obtained in the 5% Nd^{3+} doped $Ce_{0.80-x-y}Nd_xTb_yO_2$ crystal. More luminescence intensity is obtained because more oxygen ion vacancies create additional luminescent centers[28]. In addition, the smallest particle size was obtained in the 5% Nd^{3+} doped $Ce_{0.80-x-y}Nd_xTb_yO_2$ according to the FESEM analysis, the results of which are given in Fig. 4 It is a known phenomenon that decreasing the particle size increases the photoluminescence intensity[29]. At this point, it should be said that there is a concordance between the results of photoluminescence, Raman, and FESEM.

4 Conclusions

In conclusion, we observed the green photoluminescence of Tb^{3+} ions for the $Ce_{0.80-x-y}Nd_xTb_yO_2$ doped with 5%, 10% ve 15% Nd^{3+} phosphors. By doping 5% and 10% Nd^{3+} ions, we gave the same crystals red photoluminescence as well as green photoluminescence. The 5% Nd^{3+} doping was determined as the optimum doping ratio. At the same time, according to the results of the Raman analysis, the optimum doping ratio is 5% Nd^{3+}, where the maximum oxygen ion vacancy is obtained and the smallest particle size is obtained according to the FESEM analysis. According to these results, $Ce_{0.80-x-y}Nd_xTb_yO_2$ doped with 5% Nd^{3+} phosphors is a good candidate for optoelectronic applications where both red and green photoluminescence are required in the same crystal.

References

1 Bakir A H & Torun H Ö, *J Chem Soc Pak*, 43 (2021).
2 Malleshappa J, Nagabhushana H, Prasad B D, Sharma S C, Vidya Y S & Anantharaju K S, *Optik*, 127 (2016) 855.
3 Fauzi A A, Jalil A A, Hassan N S, Aziz F F A, Azami M S, Hussain I & Vo D V, *Chemosphere*, 286 (2022)131651.
4 Yan S, Liang X, Song H, Ma S & Lu Y, *Ceram Int*, 44 (2018)358.
5 Masalov A, Viagin O, Maksimchuk P, Seminko V, Bespalova I, Aslanov A & Zorenko Y, *J Lumin*, 145 (2014) 61.
6 Cabello-Guzmán G, Fernandez L, Caro-Díaz C, Lillo L, Valenzuela-Melgarejo F, Seguel M & Buono-Core G E, *Optik*, 248 (2021) 168071.
7 Kunimi S & Fujihara S, *ECS J Solid State Sci Technol*, 1 (2012) R32.
8 Fujihara S & Oikawa M, *J Appl Phys*, 95 (2004) 8002.
9 Yoshida Y & Fujihara S, *Eur J Inorg Chem*, (2011).
10 Singh V, Rathaiah M, Venkatramu V, Haase M & Kim S H, *Spectr Chimica Acta Part A: Mol Biomol Spectr*, 122 (2014) 704.
11 Balestrieri M, Colis S, Gallart M, Schmerber G, Ziegler M, Gilliot P & Dinia A, *J Mater Chem C*, 3 (2015) 7014.
12 Choudhury B & Choudhury A, *Curr Appl Phys*, 13 (2013) 217.
13 Öztürk E & Ozpozan K N, *J Therm Anal Calorim*, 117 (2014) 573.
14 Öztürk E & Sarılmaz E, *Mater Res Express*, 6 (2019) 105710.
15 Uzun E, Öztürk E & Ozpozan K N, *Luminescence*, 33 (2018) 1346.
16 Wang Z, Quan Z & Lin J, *Inorg Chem*, 46 (2007) 5237.
17 Malleshappa J, Nagabhushana H, Sharma S C, Sunitha D V, Dhananjaya N, Shivakumara C & Nagabhushana B M, *J Alloys Compd*, 590 (2014) 131.
18 Malleshappa J, Nagabhushana H, Prasad B D, Sharma S C, Vidya Y S & Anantharaju K S. Structural, *Optik*, 127 (2016) 855.
19 Shannon R D, *Acta Crystallog*, 25 (1969) 925.
20 Jamshidijam M, Thangaraj P, Akbari-Fakhrabadi A, Galeano M A N, Usuba J & Viswanathan M R, *Ceram Int*, 43 (2017) 5216.
21 Keramidas V G & White W B, *The J Chem Phys*, 59 (1973) 1561.

22 Hernández W Y, Laguna O H, Centeno M A & Odriozola J A, *J Solid State Chem*, 184 (2011) 3014.
23 He D, Hao H, Chen D, Liu J, Yu J, Lu J & Luo Y, *Catal Today*, 281 (2017) 559.
24 Öztürk E & Sarılmaz E, *Mater Chem Phys*, 239 (2020) 122085.
25 Öztürk E, Ozpozan K N & Uzun E, *J Chin Chem Soc*, 62 (2015) 47.
26 Ding L, Zhanga Q, Luo J, Liua W, Zhou W & Yin S, *J Alloys Compd*, 509 (2011) 100167.
27 Singh V, Shinde K N, Pathak M S, Singh N, Dubey V, Singh Pramod K & Jirimali H D, *Optik*, 164 (2018) 407.
28 Kostyukov A I, Zhuzhgov A V, Kaichev V V, Rastorguev A A, Snytnikov V N & Snytnikov V N, *Opt Mater*, 75 (2018) 757.
29 Kim Y & Kang S, *Acta Materialia*, 59 (2011) 3024.